Aquarius Wind Speed Products: Algorithms and Validation

Alexander G. Fore, Simon H. Yueh, *Fellow, IEEE*, Wenqing Tang, Akiko K. Hayashi, and Gary S. E. Lagerloef

***Abstract*—This paper introduces and validates the Aquarius scatterometer-only wind speed algorithm and the combined active passive (CAP) wind speed products. The scatterometer-only algorithm uses the co-polarized radar cross-section to determine the ocean surface wind speed with a maximum-likelihood estimator approach while the CAP algorithm uses both the scatterometer and radiometer channels to achieve a simultaneous ocean vector wind and sea surface salinity retrieval. We discuss complications in the speed retrieval due to the shape of the scatterometer model function at L-band and develop mitigation strategies. We find the performance of the Aquarius scatterometer-only wind speed is better than 1.00 ms^{-1}, with best performance for low wind speeds and increasing noise levels as the wind speed increases. The CAP wind speed product is significantly better than the scatterometer-only due to the inclusion of passive measurements and achieves 0.70 ms^{-1} root-mean-square error.**

***Index Terms*—Aquarius, ocean winds, radar, remote sensing, scatterometery.**

I. Introduction

AQUARIUS is a combined L-band scatterometer and radiometer designed to map the sea surface salinity (SSS) from low Earth orbit [1], [2]. It is flown on (SAC)-D which is a joint mission between the U.S. (National Aeronautics and Space Administration) and Argentina (Comisión Nacional de Actividades Espaciales). The salinity signal is detected in the radiometer due to small changes in the sea surface emissivity [3]–[5]. The effects of salinity on the surface emissivity are on the same order of magnitude as those due to surface roughness, thus accurate estimation of the surface roughness is vital to mission success. Aquarius was designed with a combined L-band scatterometer and radiometer that provide collocated roughness estimates with the radiometer brightness temperatures (T_B). The collocated scatterometer provides the estimate of surface roughness via the normalized radar cross-section (σ_0) required to isolate the salinity signal in the radiometer. The Aquarius error budget for surface roughness correction is 0.28 K [6] and recent airborne results suggest that T_B changes by about 0.33–0.34 K per ms^{-1} [7]. To meet the error requirement for the radiometer roughness correction, the scatterometer must provide an estimate of ocean surface wind speed with less than 1 ms^{-1} error.

The Aquarius scatterometer was designed to meet these needs by providing an observation of the ocean surface roughness at L-band [8]. The radiometer and scatterometer share the same antenna and have an interleaved sampling in time, thus are collocated spatially and temporally. The primary cause of ocean surface roughness is wind speed, with wave-height being a secondary effect. There is a rich heritage of Ku-band (SeaSat [9], NASA Scatterometer [10], QuikSCAT [11], and SCAT on OceanSAT-2 [12], [13]) and C-band (European Remote Sensing Satellite-1/2 [14] and Advanced Scatterometer [15]) scatterometer and model function development. However, Aquarius is the first space-borne L-band scatterometer designed to observe the ocean surface roughness. In this paper, we show that L-band provides a very capable system for retrieval of ocean surface wind speed. This is a timely observation since the upcoming Soil Moisture Active-Passive (SMAP) mission will also have a conically scanning active/passive L-band system and the capability of SMAP over the ocean is of interest to the ocean community.

In Section II we introduce the data sets considered in this study and in Section III we discuss the spatial and temporal collocation of the data considered. Next we give an overview of the model function for the scatterometer at L-band in Section IV and discuss the scatterometer-only (SCAT) and combined active passive (CAP) algorithms in Section V. Finally, we perform quantiative comparisons of the wind products in Section VI. We show that the SCAT product has root-mean-square (RMS) errors comparable to previous scatterometers and that the CAP performance is significantly better. We demonstrate that an L-band active/passive system provides good performance for ocean wind speed retrieval.

II. DataSets

We do not directly consider buoy validations due to the huge disparity in spatial sampling—the Aquarius scatterometer observes ocean surface roughness at the 100-km length scale, while the buoy observes the ocean at meter length scales. Instead we use Special Sensor Microwave Imager/Sounder (SSMI/S) as the primary reference wind speed product. Recent work [16], [17] on SSMI/S wind retrievals has ensured SSMI/S gives an intercalibrated wind product with buoys and the recently released QuikSCAT Version 3 data [11]. Thus by validating with SSMI/S we ensure consistency between passive imaging radiometers (SSMI/S and WindSAT), QuikSCAT Version 3, and buoys.

Manuscript received February 21, 2013; revised May 13, 2013; accepted June 5, 2013. Date of publication July 12, 2013; date of current version February 28, 2014.

A. G. Fore, S. H. Yueh, W. Tang, and A. K. Hayashi are with the Jet Propulsion Laboratory, California Institute of Technology, Pasadena, CA 91109 USA (e-mail: Alexander.Fore@jpl.nasa.gov).

G. S. E. Lagerloef is with Earth and Space Research, Seattle, WA 98121 USA.

Digital Object Identifier 10.1109/TGRS.2013.2267616

A. Aquarius Data

The Aquarius Level 2 (L2) data considered in this paper is version 2.0, available from the Physical Oceanography Distributed Active Archive Center at JPL. Aquarius has one scatterometer, which switches between three different push-broom antenna feeds at incidence angles of 29.4°, 38.5°, and 46.3°. Every 1.44 s, the scatterometer acquires 8 observations of the HH, HV, VH, and VV σ_0, and these 8 observations are averaged into one level 2 data block. The antenna beam footprints from each data block overlap so that every fourth block has an approximately non-overlapping footprint, however for this analysis we consider each 1.44 s data block as a separate data point.

B. SSMI/S Data

We use the SSMI/S instrument aboard Defense Meteorological Satellite Program F17 satellite. SSMI/S is a four-frequency radiometer which takes dual-polarization measurements at 19.35, 37.0, and 85.5 GHz and vertical polarization measurements at 22.235 GHz [18]. We use version 7 daily SSMI/S F17 data available from www.ssmi.com.[1] The SSMI/S daily data come on a $0.25^\circ \times 0.25^\circ$ grid with retrievals of wind speed, rain-rate, water-vapor, cloud liquid water, and time information.

C. ECMWF Data

Spatially and temporally interpolated European Centre for Medium-Range Weather Forecasts (EMCWF) operational wind data was generated for each Aquarius L2 footprint.

III. Collocation of Aquarius and SSMI/S

We constructed a global collocated data set of Aquarius and SSMI/S where every SSMI/S data point within 28 km in space and 1 h in time of the Aquarius footprint is averaged into one collocation data point. We require that scatterometer quality flag bits 31, 29, 21, and 20 are not set, indicating lack of severe RFI and no pointing errors. In addition we only consider land and ice-free data that is within $\pm 50^\circ$ latitude to remove residual ice contamination.

We obtain slightly more than 15 million collocated data points where we have ECMWF, SSMI/S, and Aquarius. In Fig. 1 we plot a map of the percentage of Aquarius data points that have a rain-free SSMI/S matchup. We see that the majority of Aquarius data have a matchup with SSMI/S, with a noticeable reduction in the tropics due to rain.

IV. Model Function

With its global L-band observations of the ocean, Aquarius has provided great insight into the radar model function. Previous estimates of the L-band model function were based on synthetic aperture radar (SAR) L-band data [19] or aircraft campaigns [7]. However, both of these have limitations, SAR instruments observe the ocean surface at far different spatial scales than Aquarius and the aircraft observations have large variation in incidence angle within the antenna beam footprint.

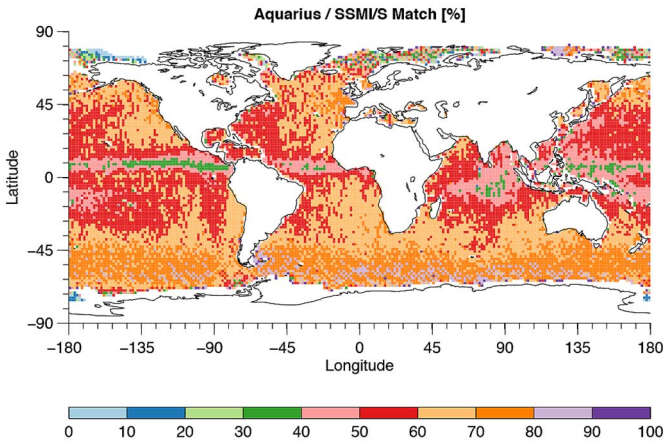

Fig. 1. Percent of Aquarius data for which there is a rain-free SSMI/S matchup.

We use a new L-band passive and active geophysical model function for ocean surface wind derived from Aquarius data [20]. In Fig. 2 we show contour plots of the Aquarius scatterometer model function for HH and VV (left to right) polarization in the top row for beam 1. In the middle and bottom rows we plot the same for beams 2 and 3, respectively. Notice that both HH and VV polarizations show far less sensitivity to the wind speed for cross-wind $(\pm 90^\circ)$ relative azimuth angles as compared to upwind/downwind relative azimuth angles (0 ± 180). This is due to the relatively large amount of azimuthal modulation for HH and VV. VV polarization, in particular, is not monotonic in the speed dimension for cross-wind values of the relative azimuth angle. The non-monotonicity of the model function in speed is clearly indicated by the closed contour on beam 2 VV polarization (second column, second row in Fig. 2).

V. Aquarius Wind Speed Retrieval Algorithms

In this section we discuss the algorithms used to retrieve the wind speed for the scatterometer-only algorithm and the CAP algorithm. Both algorithms perform a point-wise retrieval for every 1.44 s Aquarius data block.

A. Aquarius Scatterometer-Only Wind Speed

Due to the push-broom sampling of Aquarius, we have one azimuthal look with three polarizations (HH, HV, and VV) for a given spot on the ocean, however, the cross-polarization channel is not usable for non-extreme wind speeds due to the low signal-to-noise ratio. With only one azimuthal look, we cannot perform a wind vector retrieval, however, we may retrieve a wind speed if a wind direction is assumed. We use the National Centers for Environmental Prediction (NCEP) wind direction to constrain the problem, then perform a 1-D search for the best wind speed, given that wind direction and scatterometer observations. Similar to QuikSCAT, we use a

[1]SSMI/S data are produced by Remote Sensing Systems and sponsored by the NASA Earth Science MEaSUREs DISCOVER Project. Data are available at www.remss.com.

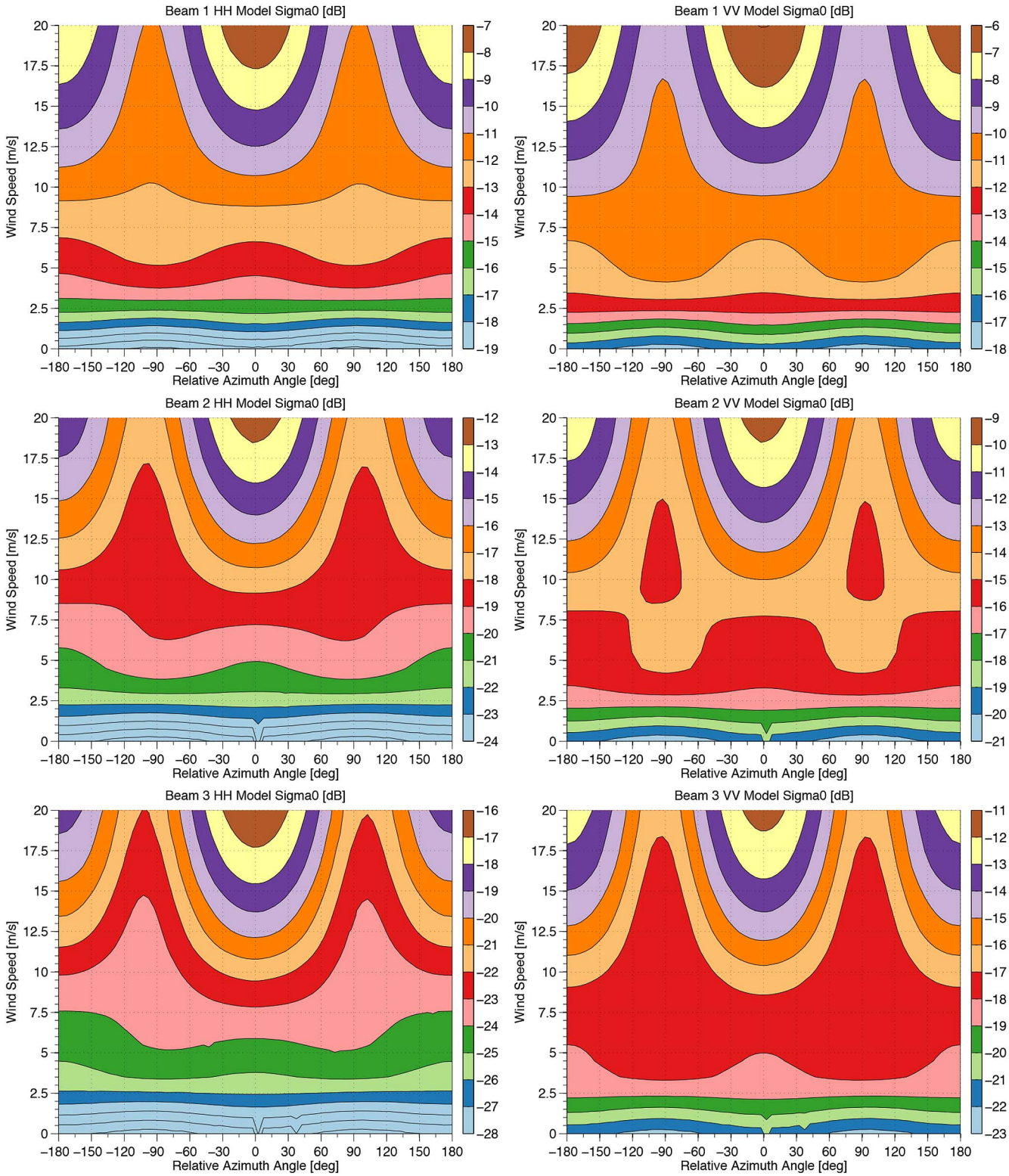

Fig. 2. Aquarius model function contour plots. In the top row we show the beam 1 HH and VV model functions from left to right. In the middle and bottom we show the same for beams 2 and 3, respectively.

maximum likelihood estimator to find the best wind speed given that wind direction, using the following cost function:

$$J = -\frac{\left(\sigma_{0,obs}^{HH} - \sigma_{0,m}^{HH}\right)^2}{\left(kp^{HH}\sigma_{0,obs}^{HH}\right)^2} - \frac{\left(\sigma_{0,obs}^{VV} - \sigma_{0,m}^{VV}\right)^2}{\left(kp^{VV}\sigma_{0,obs}^{VV}\right)^2} \quad (1)$$

where $\sigma_{0,obs}^{HH}$, $\sigma_{0,obs}^{VV}$ are the observed top-of-atmosphere (TOA) σ_0 for HH and VV polarization, $\sigma_{0,m}^{HH}$, $\sigma_{0,m}^{VV}$ are the model σ_0 for HH and VV polarization, and kp^{HH}, kp^{VV} are the estimated relative uncertainties of the observed σ_0 for HH and VV polarization. This formulation of the cost function uses both the HH and VV scatterometer observations, weighted by

the estimated uncertainly of these observations. While a total power approach would be technically invariant to the effects of Faraday rotation, the effects on the co-polarization channels are very small at L-band over ocean due to very small cross-polarizaton return relative to the co-polarization return.

Large azimuthal modulation of σ_0 at L-band causes particular relative azimuth angles to be either very flat or be non-monotonic functions of speed. The flatness and non-monotonicity of the model function shown in Fig. 2 introduces significant complications in the wind speed retrieval and we must allow for the possibility of multiple local maxima of the objective function so that we may select the best wind speed solution from these multiple local maxima. To find all the local maxima we seed the speed search at multiple initial speeds and use a line search method to find the local maxima of the objective function [21]. If multiple local maxima of the objective function in speed are found, the solution with the nearest speed to the NCEP speed is reported in the L2 data.

B. Combined Active/Passive Algorithm

The CAP algorithm is a unified sea surface salinity (SSS) and wind vector retrieval algorithm using both scatterometer and radiometer measurements [22]. The CAP cost function is

$$J_{CAP} = -\frac{(I_{obs}-I_m)^2}{\Delta I^2} - \frac{\left(\sqrt{Q_{obs}^2+U_{obs}^2}-\sqrt{Q_m^2}\right)^2}{\Delta U^2} - \frac{\left(\sigma_{0,obs}^{HH}-\sigma_{0,m}^{HH}\right)^2}{\left(kp^{HH}\sigma_{0,obs}^{HH}\right)^2} - \frac{\left(\sigma_{0,obs}^{VV}-\sigma_{0,m}^{VV}\right)^2}{\left(kp^{VV}\sigma_{0,obs}^{VV}\right)^2} - \frac{\sin^2\left[0.5(\phi-\phi_N)\right]}{0.2^2} - \frac{(w-w_N)^2}{\Delta w^2} \quad (2)$$

where $I := T_B^H + T_B^V$ is the first Stokes parameter, $Q := T_B^V - T_B^H$ is the second Stokes parameter, U is the third Stokes parameter, $\Delta I = \Delta U = 0.14$ K, ϕ is the wind direction, ϕ_N is the NCEP wind direction, w is the wind speed, w_N is the NCEP wind speed, and $\Delta w = 1.5$ m/s. Note that I_m and Q_m are functions of wind speed, relative wind direction, and SSS, whereas $\sigma_{0,m}^H H$ and $\sigma_{0,m}^V V$ are only functions of wind speed and relative wind direction. This particular formulation exploits the fact that I and $\sqrt{Q^2+U^2}$ are invariant to Faraday rotation [23]. The σ_0 are not invariant to Faraday rotation, however the effects on the co-polarization σ_0 channels are very small. The last two terms in (2) are weak constraints, the $\sin^2[0.5(\phi-\phi_N)]$ term primarily constrains the wind direction solution at low to moderate wind speeds where there is little sensitivity to wind direction. The last term improves high-wind speed performance at cross-wind relative azimuth angles.

We seed the maximum likelihood search at the ancillary SSS, NCEP wind speed, and a range of wind directions. Then we use a conjugate-gradient method to find the local maxima of the objective function in speed, direction, SSS space. Typically more than one local maxima is found and we report the ambiguity with the nearest wind direction to NCEP as the solution.

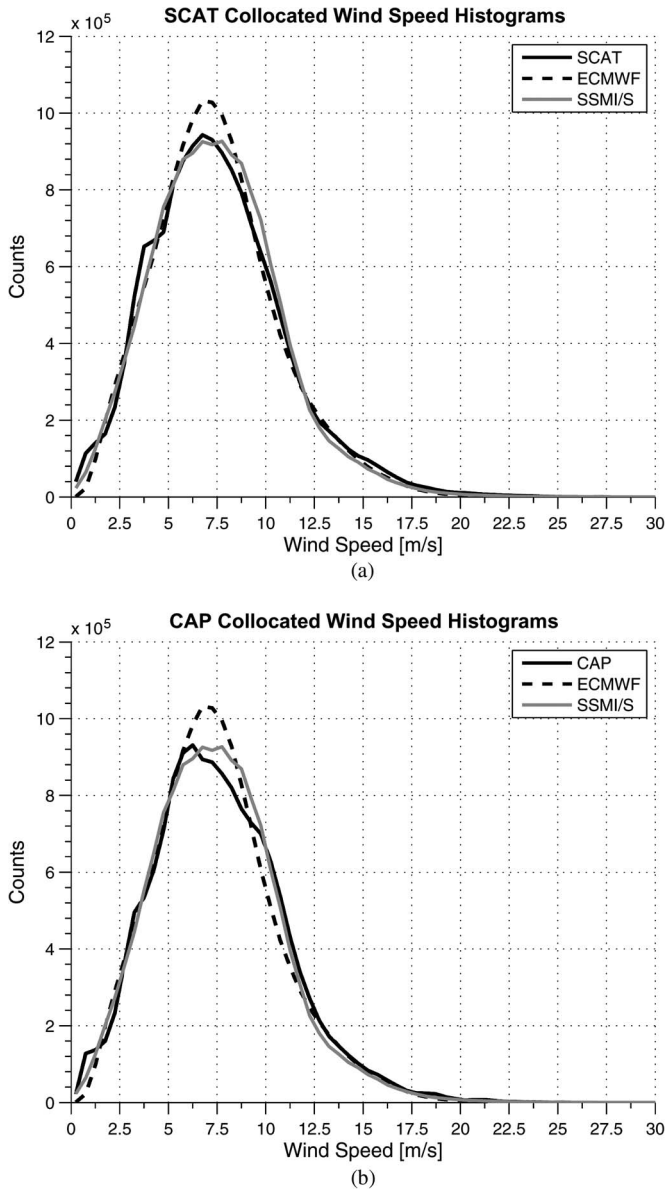

Fig. 3. Distributions of wind speed for (a) SCAT and (b) CAP (solid black line), ECMWF (dashed black line) and SSMI/S (gray line). All data are rain-free according to SSMI/S.

VI. Comparisons of Aquarius Wind Speed Products and SSMI/S Wind Speed

In Fig. 3(a) we plot histograms of SCAT and CAP (3(b)) wind speed products, SSMI/S wind speed, and ECMWF wind speed for the global collocated data set. We compute the mean and STD for each of the four wind speeds in Table I and we note that all three wind speeds have similar means and standard deviations. In Fig. 4 we show the joint distributions (log-histogram) of the two wind speed products and SSMI/S wind speeds as well as the $1:1$ line. We can clearly see some overestimation of the wind speed when SSMI/S wind speed is near 10 ms^{-1}, present in both the SCAT and CAP retrievals. This overestimation is due to the flatness of the model function in the speed direction for cross-wind relative azimuth angles, which is most significant near 10 ms^{-1}, as shown in Fig. 2.

TABLE I
AQUARIUS–SSMI/S–ECMWF GLOBAL COLLOCATION WIND SPEED MEAN AND STD

	Speed Mean	Speed STD
SCAT	7.5466	3.4480
CAP	7.6097	3.3885
SSMI/S	7.5288	3.2497
ECMWF	7.4731	3.1679

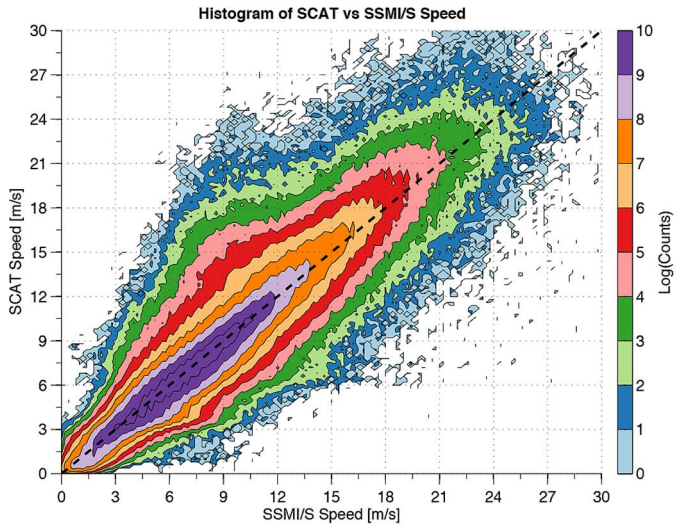

(a) SCAT Wind Speed

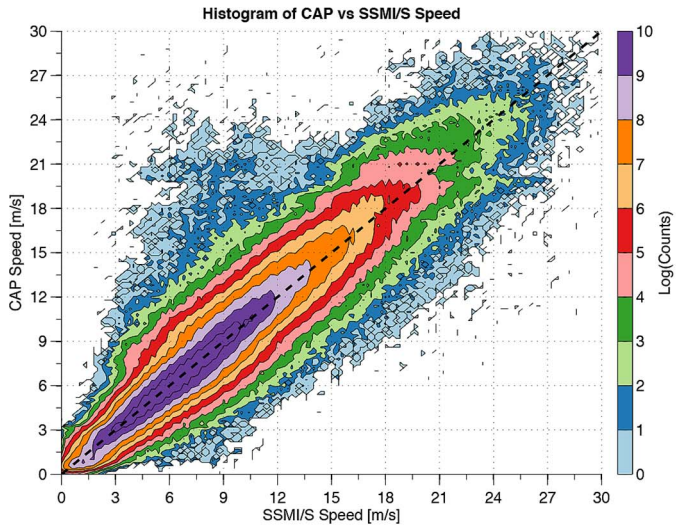

(b) CAP Wind Speed

Fig. 4. Two-dimensional histogram of collocated (a) Aquarius SCAT and SSMI/S wind speeds, and (b) CAP and SSMI/S wind speeds. Contours of the log-counts are shown as well as the 1 : 1 line.

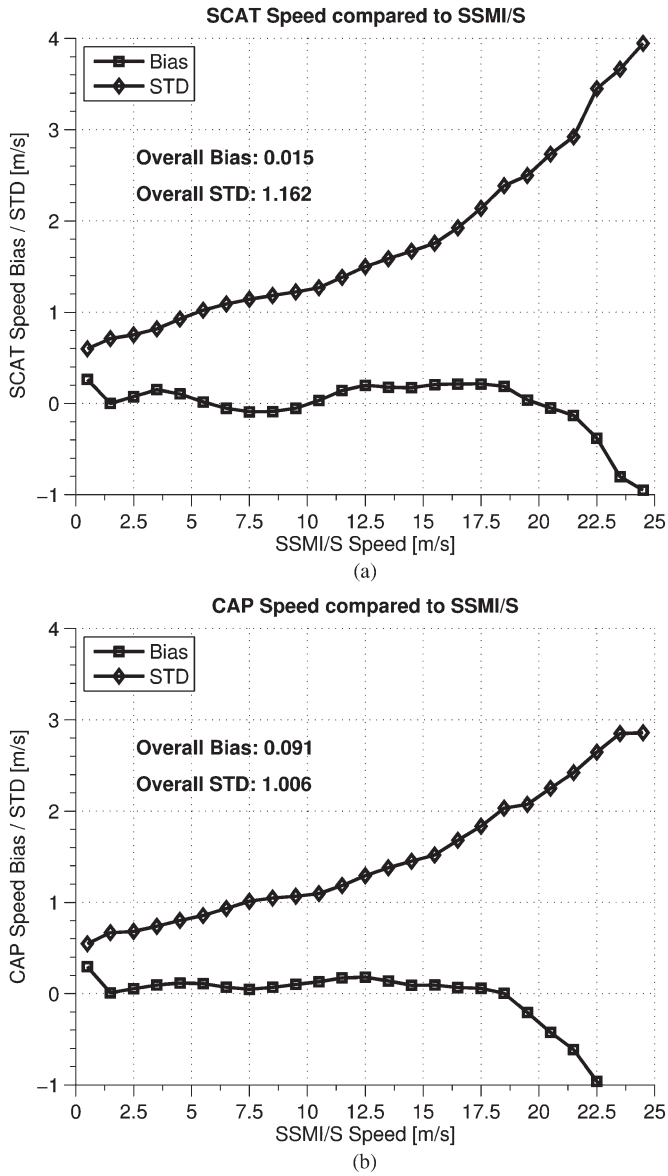

Fig. 5. (a) Conditional SCAT–SSMI/S speed mean difference and standard deviation (STD) versus SSMI/S wind speed. (b) Conditional CAP–SSMI/S speed mean difference and standard deviation (STD) versus SSMI/S wind speed. The mean difference is plotted with square markers and the STD is plotted with diamond markers. The overall speed mean difference is 0.015 m/s and the overall STD is 1.162 m/s for SCAT wind product and for CAP wind product we find 0.091 m/s mean difference and 1.006 m/s STD difference.

A. Point Comparisons

In Fig. 5(a) we plot the conditional mean and standard deviation (STD) of the Aquarius wind speed minus the SSMI/S wind speed. We see that for low wind speeds (< 5 m/s) the STD is less than 1 m/s, for 5–17 m/s the STD is between 1 and 2 m/s and for high wind speeds the STD is larger than 2 m/s. The overall speed bias is very small, 0.015 ms^{-1} and the overall speed STD is 1.162 ms^{-1}. In Fig. 5(b) we plot the same for the CAP wind speed product and the overall bias of the CAP product is 0.091 ms^{-1} and the overall CAP speed STD is 1.006 ms^{-1}. We see that the CAP speed STD is improved as compared to the scatterometer-only wind speed across the SSMI/S speed range and much improved at wind speeds larger than 17.5 m/s. The improvement in the CAP wind speed performance at higher wind speeds is due to the inclusion of the radiometer measurements. At high wind speeds the scatterometer-only performance is degraded at crosswind relative azimuth angles due to the nearly flat curve of σ_0 versus wind speed.

TABLE II
SCAT TRIPLE-COLLOCATION RESULTS

	SSMI/S	ECMWF	SCAT
Bias	0	0.2461	-0.3250
Slope	1	0.9599	1.0454
RMS Error	0.6801	0.8544	0.9357
	SSMI/S	**QuikSCAT**	**SCAT**
Bias	0	0.4901	0.0247
Slope	1	0.9475	1.0174
RMS Error	0.6374	0.9553	0.9833

TABLE III
CAP TRIPLE-COLLOCATION RESULTS

	SSMI/S	ECMWF	CAP
Bias	0	0.2126	-0.2679
Slope	1	0.9644	1.0465
RMS Error	0.7133	0.8290	0.6967
	SSMI/S	**QuikSCAT**	**CAP**
Bias	0	0.4819	-0.0071
Slope	1	0.9487	1.0219
RMS Error	0.6466	0.9497	0.7072

B. Triple Collocation

Following [24]–[26] we perform a triple-collocation analysis of the Aquarius SCAT/ECMWF/SSMI/S and CAP/ECMWF/SSMI/S data sets. We assume the following error model for each of the three wind data sets:

$$\begin{aligned} w_A^i &= \alpha_A + \beta_A W^i + r_A^i \\ w_E^i &= \alpha_E + \beta_E W^i + r_E^i \\ w_S^i &= \alpha_S + \beta_S W^i + r_S^i \end{aligned} \tag{3}$$

where the subscripts A, E, S correspond to Aquarius, ECMWF and SSMI/S, respectively, α is the bias of each, β is the scale error for each, and r^i is the RMS error associated with each for true wind w^i. We assume that the RMS errors are zero-mean, i.e., $\langle r_A^i \rangle = \langle r_E^i \rangle = \langle r_S^i \rangle = 0$, and that the errors are not correlated, i.e., $\langle r_A^i r_E^i \rangle = \langle r_A^i r_S^i \rangle = \langle r_E^i r_S^i \rangle = 0$, where angle brackets indicate averaging. To solve these equations, we must choose one wind product to have zero bias and unity slope, in this analysis we choose SSMI/S. Then we introduce

$$\begin{aligned} w_A^{*,i} &= w_A^i - \langle w_A^i \rangle = \beta_A W^i + r_A^i \\ w_E^{*,i} &= w_E^i - \langle w_E^i \rangle = \beta_E W^i + r_E^i \\ w_S^{*,i} &= w_S^i - \langle w_S^i \rangle = W^i + r_S^i. \end{aligned} \tag{4}$$

We find $\beta_A = \langle w_A^{*,i} w_E^{*,i} \rangle / \langle w_E^{*,i} w_S^{*,i} \rangle$ and $\beta_E = \langle w_A^{*,i} w_E^{*,i} \rangle / \langle w_A^{*,i} w_S^{*,i} \rangle$. Next we write

$$\begin{aligned} \hat{w}_A^i &= w_A^{*,i} / \beta_A = W^i + \hat{r}_A^i \\ \hat{w}_E^i &= w_E^{*,i} / \beta_E = W^i + \hat{r}_E^i \\ \hat{w}_S^i &= w_S^{*,i} / \beta_S = W^i + \hat{r}_S^i \end{aligned} \tag{5}$$

where $\hat{r}_A^i = r_A^i / \beta_A$, $\hat{r}_E^i = r_E^i / \beta_N$, and $\hat{r}_S^i = r_S^i / \beta_S$. Then by averaging the three cross-products of $\{\hat{w}_A^i, \hat{w}_E^i, \hat{w}_S^i\}$ we may solve for the bias, slope, and RMS errors of each. In Table II we show the results of the triple-collocation analysis for the SCAT wind product and in Table III the same for the CAP product. We have also performed a triple-collocation analysis using Aquarius SCAT/QuikSCAT/SSMI/S and CAP/QuikSCAT/SSMI/S to alleviate concerns of correlations between the three data sets. We collocated all land/ice/rain free QuikSCAT observations that were within 25 km and 60 min of the Aquarius footprint, in a similar was as with SSMI/S. These results are included in Tables II and III, and give fairly consistent results to the Aquarius/SSMI/S/ECMWF analysis. Compared to QuikSCAT, we find that the Aquarius SCAT product is slightly worse by about 0.03 ms^{-1} and the CAP product is significantly better than that from QuikSCAT, by 0.24 ms^{-1}.

These two analysis show that ECMWF has an RMS error around 0.83 to 0.85 ms^{-1}, SSMI/S has an RMS error around 0.63 to 0.71 ms^{-1}, and QuikSCAT has an RMS error around 0.95 ms^{-1}. The SCAT product is found to have an RMS error of 0.94 to 0.98 ms^{-1} and the CAP product is found to have and RMS error of 0.70 ms^{-1}. While all the results from the various analysis are not the same, they are all in reasonable agreement with each other. These results give the partition of the error between SSMI/S and the SCAT/CAP wind speed product shown in 5.

VII. SUMMARY

We have undertaken a comprehensive comparison of Aquarius scatterometer-only wind speed retrievals to SSMI/S. We find that the SCAT product gives speed retrievals with very small bias up to 20 ms^{-1}, and has RMS errors of less than 1 ms^{-1}. This performance is comparable with QuikSCAT [11], SCAT on OceanSAT-2, and Advanced Scatterometer [25]). The STD increases with increasing wind speed due to the large azimuthal modulation in the model function for the co-polarization channels. This gives regions of relative azimuth angles where the model function is fairly "flat" in the speed dimension. When the passive brightness temperatures are used as well in the CAP product, the high wind speed performance is significantly better and we achieve RMS errors of 0.70 ms^{-1}. The radiometer model function does not display the same flatness at crosswind as the scatterometer model function, and this is the main reason for the better performance of the CAP wind speed product as compared to the SCAT product. Finally, the inclusion of a cross-polarization channel with good SNR would significantly improve the active-only products since it does not display the same flatness as the co-polarization channels. Aquarius has proven that an L-band active/passive system can give good wind speed retrievals, and we expect that SMAP will make a significantly better system for ocean vector winds due to the additional azimuth look and increased swath width.

ACKNOWLEDGMENT

This research was carried out at the Jet Propulsion Laboratory, California Institute of Technology, under a contract with the National Aeronautics and Space Administration.

REFERENCES

[1] G. Lagerloef, F. R. Colomb, D. Le Vine, F. Wentz, S. Yueh, C. Ruf, J. Lilly, J. Gunn, Y. Chao, A. deCharon, G. Feldman, and C. Swift, "The Aquarius/SAC-D mission: Designed to meet the salinity remote-sensing challenge," *Oceanography*, vol. 21, no. 1, pp. 68–81, Mar. 2008.

[2] D. Le Vine, G. Lagerloef, F. Colomb, S. Yueh, and F. Pellerano, "Aquarius: An instrument to monitor sea surface salinity from space," *IEEE Trans. Geosci. Remote Sens.*, vol. 45, no. 7, pp. 2040–2050, Jul. 2007.

[3] L. Klein and C. Swift, "An improved model for the dielectric constant of sea water at microwave frequencies," *IEEE Trans. Antennas Propag.*, vol. AP-25, no. 1, pp. 104–111, Jan. 1977.

[4] T. Meissner and F. Wentz, "The complex dielectric constant of pure and sea water from microwave satellite observations," *IEEE Trans. Geosci. Remote Sens.*, vol. 42, no. 9, pp. 1836–1849, Sep. 2004.

[5] W. Wilson, S. Yueh, S. Dinardo, and F. Li, "High-stability L-band radiometer measurements of saltwater," *IEEE Trans. Geosci. Remote Sens.*, vol. 42, no. 9, pp. 1829–1835, Sep. 2004.

[6] Y. Chao, "L2A Aquarius science requirements," Jet Propulsion Lab., Pasadena, CA, USA, JPL D-29054, Jul. 2008.

[7] S. H. Yueh, S. J. Dinardo, A. G. Fore, and F. K. Li, "Passive and active L-band microwave observations and modeling of ocean surface winds," *IEEE Trans. Geosci. Remote Sens.*, vol. 48, no. 4, pp. 3087–3100, Aug. 2010.

[8] A. Freedman, D. McWatters, and M. Spencer, "The Aquarius scatterometer: An active system for measuring surface roughness for sea-surface brightness temperature correction," in *Proc. IEEE IGARSS*, Aug. 2006, pp. 1685–1688.

[9] W. L. Jones, L. C. Schroeder, D. H. Boggs, E. M. Bracalente, R. A. Brown, G. J. Dome, W. J. Pierson, and F. J. Wentz, "The SEASAT-A satellite scatterometer: The geophysical evaluation of remotely sensed wind vectors over the ocean," *J. Geophys. Res.*, vol. 87, no. C5, pp. 3297–3317, Apr. 1982.

[10] F. Naderi, M. Freilich, and D. Long, "Spaceborne radar measurement of wind velocity over the ocean-an overview of the NSCAT scatterometer system," *Proc. IEEE*, vol. 79, no. 6, pp. 850–866, Jun. 1991.

[11] A. G. Fore, B. W. Stiles, A. H. Chau, B. A. Williams, R. S. Dunbar, and E. Rodríguez, "Point-wise wind retrieval and ambiguity removal improvements for the QuikSCAT climatological data set," *IEEE Trans. Geosci. Remote Sens.*, vol. 52, no. 1, pp. 51–59, Jan. 2014.

[12] B. Gohil, P. Sharma, R. Sikhakolli, and A. Sarkar, "Directional Stability and Conservation of Scattering (DiSCS)-based directional-ambiguity removal algorithm for improving wind fields from scatterometer: A QuikSCAT example," *IEEE Geosci. Remote Sens. Lett.*, vol. 7, no. 3, pp. 592–595, Jul. 2010.

[13] B. Gohil, A. Sarkar, and V. Agarwal, "A new algorithm for wind-vector retrieval from scatterometers," *IEEE Geosci. Remote Sens. Lett.*, vol. 5, no. 3, pp. 387–391, Jul. 2008.

[14] E. Attema, "The active microwave instrument on-board the ERS-1 satellite," *Proc. IEEE*, vol. 79, no. 6, pp. 791–799, Jun. 1991.

[15] J. Figa-Saldaña, J. J. Wilson, E. Attema, R. Gelsthorpe, M. R. Drinkwater, and A. Stoffelen, "The Advanced Scatterometer (ASCAT) on the Meteorological Operational (MetOp) platform: A follow on for European wind scatterometers," *Can. J. Remote Sens.*, vol. 28, no. 3, pp. 404–412, Jun. 2002.

[16] L. Ricciardulli and F. Wentz, "Reprocessed QuikSCAT (V04) wind vectors with Ku-2011 geophysical model function," Remote Sens. Syst., Santa Rosa, CA, USA, Tech. Rep. 043011, Apr. 2011.

[17] T. Meissner, L. Ricciardulli, and F. Wentz, "All-weather wind vector measurements from intercalibrated active and passive microwave satellite sensors," in *Proc. IEEE Int. Geosci. Remote Sens. Symp.*, Jul. 2011, pp. 1509–1511.

[18] F. J. Wentz, "A well-calibrated ocean algorithm for special sensor microwave/imager," *J. Geophys. Res.*, vol. 102, no. C4, pp. 8703–8718, Apr. 1997.

[19] O. Isoguchi and M. Shimada, "An L-band ocean geophysical model function derived from PALSAR," *IEEE Trans. Geosci. Remote Sens.*, vol. 47, no. 7, pp. 1925–1936, Jul. 2009.

[20] S. H. Yueh, W. Tang, A. G. Fore, G. Neumann, A. Hayashi, A. Freedman, J. Chaubell, and G. Lagerloef, "L-band passive and active microwave geophysical model functions of ocean surface winds and applications to Aquarius retrieval," *IEEE Trans. Geosci. Remote Sens.*, vol. 51, no. 9, pp. 4619–4632, Sep. 2013.

[21] R. Dunbar, S. Hsiao, Y. Kim, K. S. Pak, B. H. Weiss, and A. Zhang, "Science algorithm specification for SeaWinds on QuikSCAT and SeaWinds on ADEOS-II," Jet Propulsion Lab., Pasadena, CA, USA, Oct. 2001.

[22] S. Yueh and J. Chaubell, "Sea surface salinity and wind retrieval using combined passive and active L-band microwave observations," *IEEE Trans. Geosci. Remote Sens.*, vol. 50, no. 4, pp. 1022–1032, Apr. 2012.

[23] S. Yueh, "Estimates of Faraday rotation with passive microwave polarimetry for microwave remote sensing of earth surfaces," *IEEE Trans. Geosci. Remote Sens.*, vol. 38, no. 5, pp. 2434–2438, Sep. 2000.

[24] A. Stoffelen, "Toward the true near-surface wind speed: Error modeling and calibration using triple collocation," *J. Geophys. Res.–Oceans*, vol. 103, no. C4, pp. 7755–7766, Apr. 1998.

[25] J. Vogelzang, A. Stoffelen, A. Verhoef, and J. Figa-Saldaña, "On the quality of high-resolution scatterometer winds," *J. Geophys. Res.*, vol. 116, no. C10, p. C10033, Oct. 2011.

[26] D. Leroux, Y. Kerr, P. Richaume, and B. Berthelot, "Estimating SMOS error structure using triple collocation," in *Proc. IEEE IGARSS*, Jul. 2011, pp. 24–27.

Alexander G. Fore received the A.B. degree in physics from Vassar College, Poughkeepsie, NY, USA, in 2002, and the M.S. and Ph.D. degrees in physics from Carnegie Mellon University, Pittsburgh, PA, USA, in 2004 and 2008, respectively. His doctoral work was modeling of complex fluids using the Lattice Boltzmann method.

In March 2008 he joined the Radar Science and Engineering section at the Jet Propulsion Laboratory (JPL), Pasadena, CA, USA. At JPL he has been working primarily on scatterometry, both forward modeling of the radar observation as well as retrieval of the geophysical quantity from radar observation. He has also has experience in synthetic aperture radar processing and calibration algorithms.

Simon H. Yueh (F'09) received the Ph.D. degree in electrical engineering in January 1991 from the Massachusetts Institute of Technology, Cambridge, MA, USA.

He was a Postdoctoral Research Associate at the Massachusetts Institute of Technology from February to August 1991. In September 1991, he joined the Radar Science and Engineering Section at the Jet Propulsion Laboratory (JPL), Pasadena, CA, USA. He was the Supervisor of the radar system engineering and algorithm development group from 2002 to 2007. He was the Deputy Manager of Climate, Oceans and Solid Earth section from July 2007 to March 2009, and the Section Manager from April 2009 to January 2013. He was also the Project Scientist of the National Aeronautics and Space Administration (NASA) Aquarius mission for global sea surface salinity observations from January 2012 to September 2013. He has become the Project Scientist of NASA Soil Moisture Active Passive Mission since October 2013. He has been the Principal/Co-Investigator of numerous research projects, including the polarimetric wind radiometer research; airborne scatterometer project for hurricane wind measurements; Passive/Active L-band Sensor (PALS) project; NASA Instrument Incubator Project for a mission concept using a large mesh-deployable antenna for soil moisture and ocean salinity sensing; the airborne polarimetric radar (POLSCAT) for ocean wind velocity measurements; the POLSCAT/Cold Land Processes Experiments (CLPX-1 and -2) in 2002–2004 and 2006–2008; the Advanced Component Technology lightweight dual-frequency antenna feed project; the Aquarius PALS High Wind Campaign in 2009; the POLSCAT-CLPX3 experiment in 2009–2010. He has authored four book chapters and published more than 150 publications and presentations.

Dr. Yueh received the 2009 IEEE GRSS Transaction Prize Paper award, 2002 IEEE GRSS Transaction Prize Paper award, the 2000 Best Paper Award in the IEEE International Geoscience and Remote Symposium 2000, and the 1995 IEEE GRSS Transaction Prize Paper award for a paper on polarimetric radiometry. He received the JPL Lew Allen Award in 1998 and Ed Stone Award in 2003. He is an Associate Editor of the IEEE TRANSACTIONS ON GEOSCIENCE AND REMOTE SENSING.

Wenqing Tang received the Ph.D. degree in physics from the Michigan State University, East Lansing, MI, USA, in July 1987.

In October 1989, she joined the Climate, Oceans and Solid Earth section, Jet Propulsion Laboratory (JPL), California Institute of Technology, Pasadena, CA, USA. She has been working on scientific data analysis and retrieval algorithm development of satellite earth remote sensing data. She has been the Co-Investigator of many research projects, including the NASA Ocean Vector Wind Science Team (OVWST) on SeaWinds scatterometers NSCAT and QuikSCAT; the NASA Global Precipitation Measurement (GPM) mission; the NASA Energy and Water cycle Study (NEWS); and she was the Principal Investigator of the project producing global ocean surface vector wind fields and related geophysical parameters from spacebased sensors under NOAA Climate and Global Change Program Directed at Climate Change Data and Detection/Enhanced Data Sets. She joined the Aquarius post-launch instrument calibration and validation team in 2011 and has been working on Aquarius radar/radiometer geophysical model functions and other research activities including the rain effect on roughness correction to improve sea surface salinity retrieval.

Akiko K. Hayashi received the B.S. degree in civil engineering and the M.S. degree in structural engineering at Duke University, Durham, NC, USA. After graduating, she came to Jet Propulsion Laboratory in Pasadena, CA, USA, to work in the Structures and Dynamics Technology Group doing structural analysis and finite element modeling. In 1988, she moved to the Oceanography Group, where she started working on altimetry data from GEOSAT. She is currently working on altimetry data from OSTM/Jason-2 and ocean salinity data from Aquarius.

Gary S. E. Lagerloef received the Ph.D. degree in physical oceanography from the University of Washington, Seattle, WA, USA, in 1984.

He currently serves as a Principal Investigator of the NASA Aquarius Mission to study the interactions between the Earth's water cycle, ocean circulation, and climate. He has served on numerous science teams and working groups over the past 20 years, which include the Salinity Sea Ice Working Group (Chair), Satellite Altimeter Requirements for Climate Research Working Group (Cochair), NRC Committee on Earth Gravity Measurements from Space, the AMS Committee on Sea Air Interaction and on NASA Science Working Teams for Topex/Poseidon/Jason missions, Ocean Vector Winds, and the Tropical Rainfall Measurement Mission. He worked with Science Applications International Corporation, and was the NASA Physical Oceanography Program Manager from 1988 to 1990. He has served in the NOAA Commissioned Officer Corps and in the U.S. Coast Guard. Currently, he is with Earth and Space Research, Seattle, which he co-founded in 1995. He is the author of over 60 publications and presentations. He has been a Guest Editor for the *Journal of Geophysical Research—Oceans* and is a member of several professional associations, learned, and technical societies. His research interests include ocean circulation and climate dynamics with special emphasis in developing new applications for satellite remote sensing.